Optical properties of ice particles in young contrails

Gang Hong [a,*], Qian Feng [a], Ping Yang [a], George W. Kattawar [a], Patrick Minnis [b], Yong X. Hu [b]

[a] *Department of Atmospheric Sciences, Texas A&M University, College Station, TX 77843, USA*
[b] *NASA Langley Research Center, Hampton, VA 23681, USA*

A B S T R A C T

The single-scattering properties of four types of ice crystals (pure ice crystals, ice crystals with an internal mixture of ice and black carbon, ice crystals coated with black carbon, and soot coated with ice) in young contrails are investigated at wavelengths 0.65 and 2.13 μm using Mie codes for coated spheres. The four types of ice crystals show differences in their single-scattering properties because of the embedded black carbon whose volume ratio is assumed to be 5%. The bulk-scattering properties of young contrails consisting of the four types of ice crystals are further investigated by averaging their single-scattering properties over a typical ice particle size distribution found in young contrails. The effect of the radiative properties of the four types of ice particles on the Stokes parameters I, Q, U, and V is also investigated for different viewing zenith angles and relative azimuth angles with a solar zenith angle of 30° using a vector radiative transfer model based on the adding-doubling technique. The Stokes parameters at a wavelength of 0.65 μm show pronounced differences for the four types of ice crystals, whereas the counterparts at a wavelength of 2.13 μm show similar variations with the viewing zenith angle and relative azimuth angle. However, the values of the results for the two wavelengths are noticeably different.

© 2008 Elsevier Ltd. All rights reserved.

1. Introduction

Contrails generated from high-altitude aircraft exhaust may be potentially important for climate study on both regional and global scales [1–6]. The impact of contrails and contrail-induced cirrus on the terrestrial climate system is likely to become more prominent, as air traffic increases 2–5% annually [2,3]. Characterization of contrail particles and of their transition into aged contrails and cirrus clouds is an important step in assessing the global impact of aircraft emissions on climate [7]. Theoretical simulations and laboratory measurements have been carried out for the formation and evolution of contrails [8,9,17]. The microphysical and optical properties of contrails have been also extensively studied by using optics-based in-situ and remote-sensing methods [10–15], which need the knowledge of the single-scattering properties of contrail particles.

The microphysical and optical properties of contrails and contrail-induced cirrus clouds are quite different from those of natural cirrus clouds [11,12,14–18]. Unlike a natural cirrus cloud within which ice crystals have a wide size spectrum, a contrail usually has a higher number concentration of small ice crystals [5,11,13,14,17,19]. During the transition of contrails into cirrus clouds, the ice crystal size increases and the corresponding number concentration decreases, as articulated by Schörder et al.[17], who analyzed the microphysical properties of contrails and contrail-induced cirrus clouds observed

---

* Corresponding author. Tel.: +1 979 845 5008.
  E-mail address: hong@ariel.met.tamu.edu (G. Hong).

during 15 airborne missions over central Europe. It is there found that contrails are dominated by high concentrations ($> 100 \, \mathrm{cm}^{-3}$) of quasi-spherical ice crystals (i.e., droxtals) with mean diameters in the range of 1–10 μm. Larger ice crystals in the range 10–20 μm with typical concentrations 2–5 cm^{-3} are found in young contrail-cirrus clouds that consist mostly of regularly-shaped ice crystals.

Contrail particles have been found to contain soot, i.e., black carbon [12,14–16]. The scattering and radiative properties of soot have been extensively studied e.g., [20–25] because soot plays a significant role in the absorption of solar radiation by atmospheric aerosols. The effect of black carbon on the scattering and absorption of solar radiation by cloud droplets has been investigated for almost four decades [26–32]. Soot, either as an external attachment or as an internal inclusion, changes the refractive index of ice particles [15,16,31,33], and influences the scattering properties of ice particles.

The influence of soot inclusions on the visible and infrared radiative properties of ice crystals has not been extensively investigated. Macke et al. [31] examined the influence for large ice particles at visible wavelengths. Chylek and Hallett [16] showed that the effect of soot on the optical properties of contrail particles depends on the type of external or internal mixing and the volume fraction of soot. Kuhn et al. [15] found a mixture of pure ice particles, black carbon aerosol, and an internal mixture of these components in the contrails using the measurements acquired during the SULFUR-4 experiment in March 1996 over southern Germany. In their findings, the volume fraction of the black carbon attached to or included within ice crystals was approximately 15–20%. Furthermore, the contrail was found to be a mixture of 15% ice particles, 32% ice with black carbon, and 24% black carbon, and 29% unknown aerosols. These results derived for a young contrail well illustrates the importance of knowing the composition of contrail particles so that the optical properties (e.g., refractive indices) of these particles can be derived.

A black-carbon-volume-ratio (BCVR) of 15–20%, which was observed by Kuhn et al. [15], is limited for particles with an average diameter of 0.5 μm. The value of the BCVR becomes much smaller (less than 1%) when ice particles become larger [34]. The value of the BCVR also varies with the sizes of ice particles and there is no commonly accepted value of the BCVR for young contrail particles. In the present study, a BCVR of 5% is assumed in order to simplify the simulations.

In the present study, the optical properties of four types of ice crystals, namely pure ice crystals, ice crystals with an internal mixture of ice and black carbon, ice crystals coated with black carbon, and soot coated with ice, are investigated at wavelengths 0.65 and 2.13 μm. The rest of this paper is organized as follows. Section 2 presents the aforementioned four ice crystal models. Additionally, in Section 2 a Mie scattering program for coated spheres and a vector radiative transfer model used, respectively, for the present single-scattering and radiative transfer simulations are also briefly described. Section 3 presents the single-scattering properties and bulk optical properties of the contrail particles and the simulation of the Stokes parameters associated with contrails. Finally, the summary is given in Section 4.
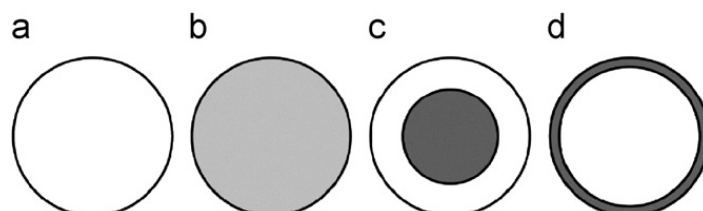
Fig. 1. Four types of ice particles in young contrails used in the present study. (a) Pure ice paticle, (b) representing the internal mixture of ice and black carbon, (c) coated soot with ice, (d) coated ice with black carbon. The volume mixing ratio of black carbon in (b–d) is assumed to be 5% in the present study.

Table 1
Refractive indexes of ice particles considered in the present study

Ice particle	Wavelength (μm)	Refractive index
	0.65 2.13	1.30804+1.4325E−08i 1.26732+5.5682E−04i
	0.65 2.13	1.33014+0.02150i 1.29421+0.02529i
	0.65 2.13	1.75000+0.43000i[a] 1.80520+0.49520i[a]
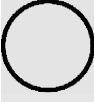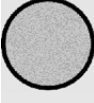
[a] For black carbon in core or shell.
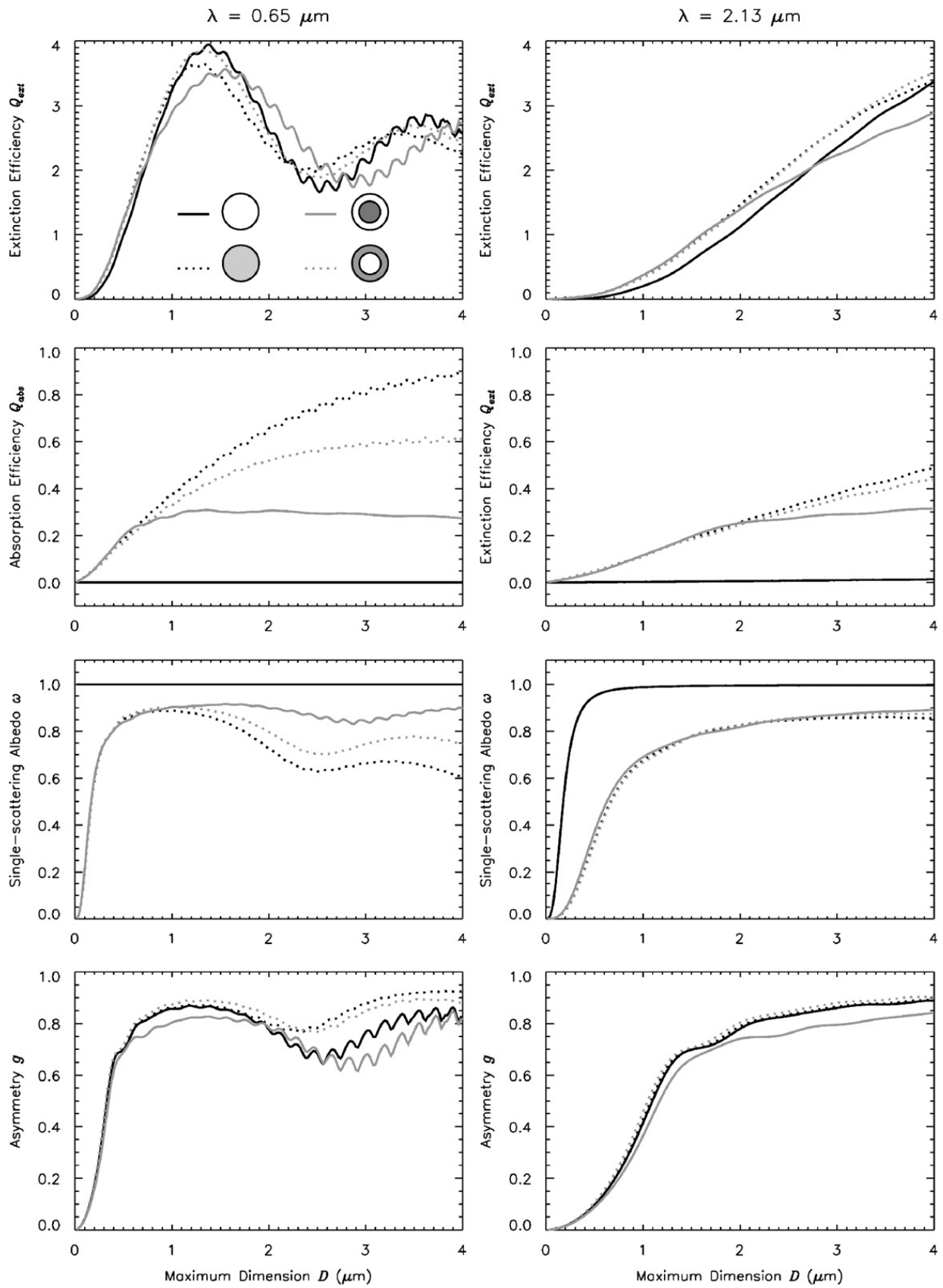
Fig. 2. Single-scattering properties (extinction efficiency Q_{ext}, absorption efficiency Q_{abs}, single-scatting albedo ω, and asymmetry factor g) of ice particles in young contrails.

2. Methodology

2.1. Ice crystal models

A large number concentration with small ice crystals is generally observed in contrails e.g., [5,11,13,14,17,19]. These ice particles in contrails have been found to be quasi-spherical [17]. Additionally, the external and internal mixtures of black carbon and ice crystals have been found in young contrails [15,16].

Four types of ice crystals found in young contrails used in the present study are shown in Fig. 1. The pure ice particle (Fig. 1a) is composed of pure ice. The particles with internal mixtures of ice and black carbon are typically represented for contrail particles (Fig. 1b) and, hereafter, are denoted as contrail particles. In this study, a BCVR of 5% is used for contrail particles, soot coated with pure ice (Fig. 1c), and ice particles coated with black carbon (Fig. 1d).

The refractive index of pure ice is from Warren [35]. The black carbon refractive index is from the database of Levoni et al. [36]. The mean refractive index of a contrail particle, m, can be calculated as follows [36]:

$$m = \frac{v_i m_i + v_b m_b}{v_i + v_b} \tag{1}$$

where m_i and m_b are the refractive indexes of pure ice and black carbon, respectively, v_i and v_b are the volume mixing ratios of pure ice and black carbon, respectively. The refractive indexes of the four types of ice crystals are given in Table 1.

2.2. Mie code for coated spheres

The conventional Lorenz–Mie formalism has been extended to study the scattering properties of coated spheres e.g., [33,37–43]. A standard code, DMiLay.f, developed by Warren Wiscombe (NASA Goddard Space Flight Center) is used in
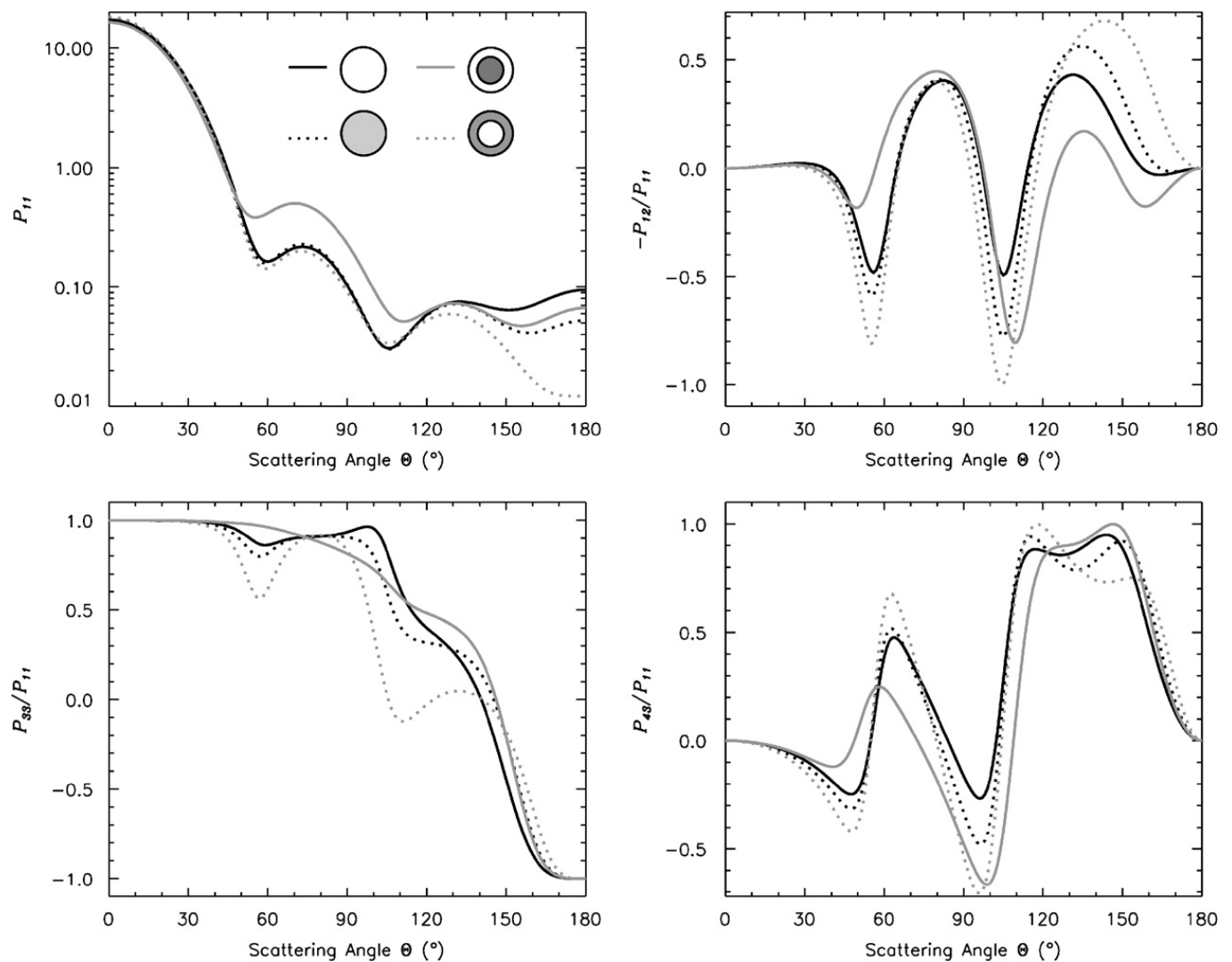
Fig. 3. Phase matrix as a function of scattering angle at 0.65 μm with a size parameter of 4.0 for ice particles in young contrails.

this study for Mie calculations for coated spheres. DMLay.f is a double-precision version of MieLay.f, which is based on the formulas presented in Toon and Ackerman [38]. The Mie code for coated spheres is available at http://atol.ucsd.edu/scatlib/ codes2/wiscombe.zip. Ice crystals in young contrails are quasi-spheres [7,17]. Thus, as a first-order approximation, in this study we assume that the overall shapes of young contrail particles are ice spheres. With this simplification, the phase matrix $\mathbf{P}(\cos \Theta)$ has only four independent matrix elements as follows [44]:

$$\mathbf{P}(\cos \Theta) = \begin{bmatrix} P_{11} & P_{12} & 0 & 0 \\ P_{12} & P_{11} & 0 & 0 \\ 0 & 0 & P_{33} & P_{34} \\ 0 & 0 & -P_{34} & P_{33} \end{bmatrix} \tag{2}$$

Note that nonsphericity of contrail particles may substantially alter the full scattering phase matrix e.g., [45–47].

2.3. Vector radiative transfer model

A number of vector radiative transfer models have been developed on the basis of different techniques, including the Monte Carlo method [48,49], the adding-doubling model [50–52], and the vector discrete-ordinates method [53–55], and the successive-orders-of-scattering method [56].

In this study, the vector radiative transfer model developed by [51] on the basis of the adding-doubling method is employed to simulate the full Stokes parameters for contrails that are assumed to be vertically inhomogeneous. This vector radiative transfer model is suitable for simulating radiation at solar wavelengths. In this model, the six independent matrix elements of the phase matrix in Eq. (2) are taken into account. The details of this vector radiative transfer computational package were documented by [51].
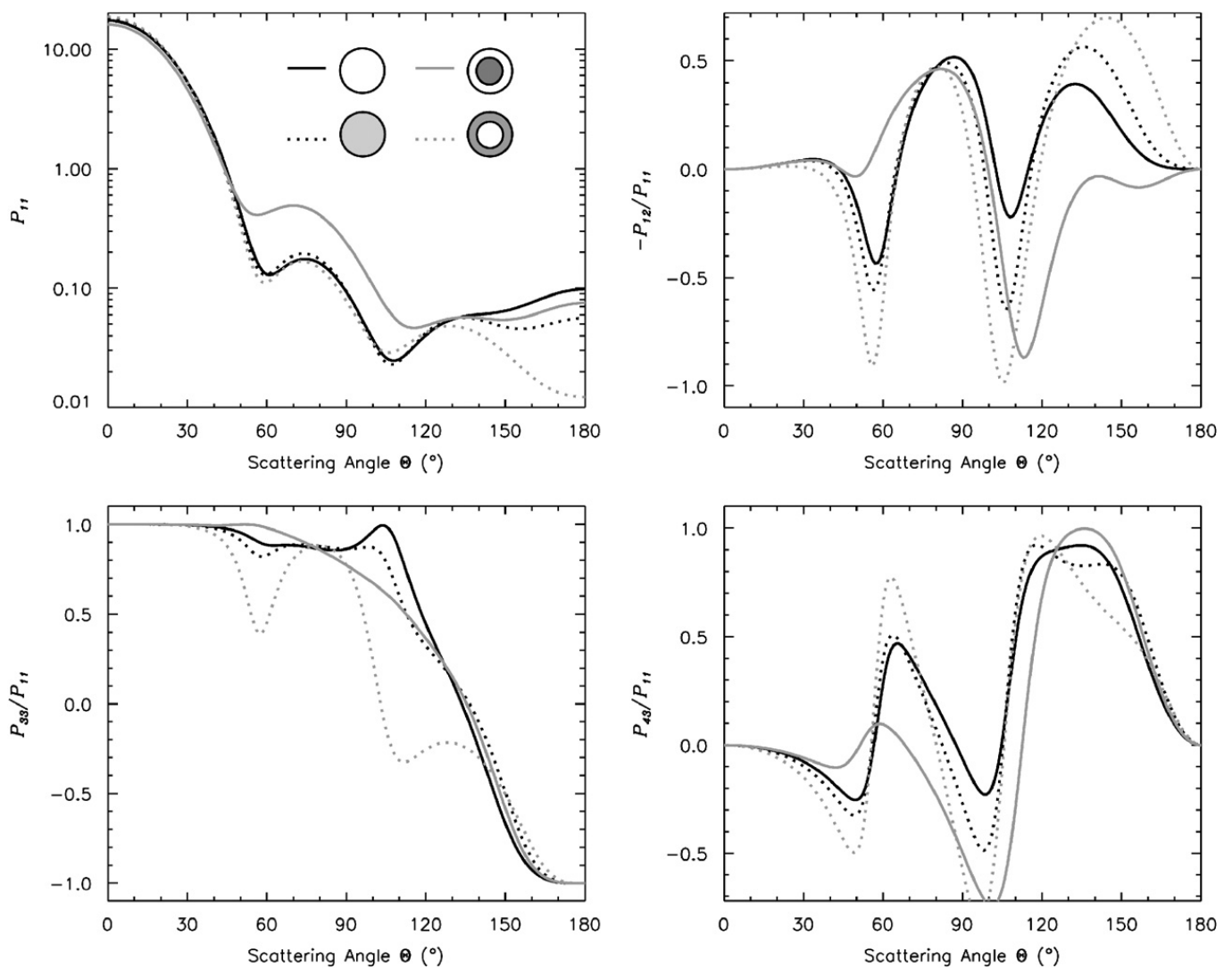
Fig. 4. Same as Fig. 3, but for 2.13 μm.
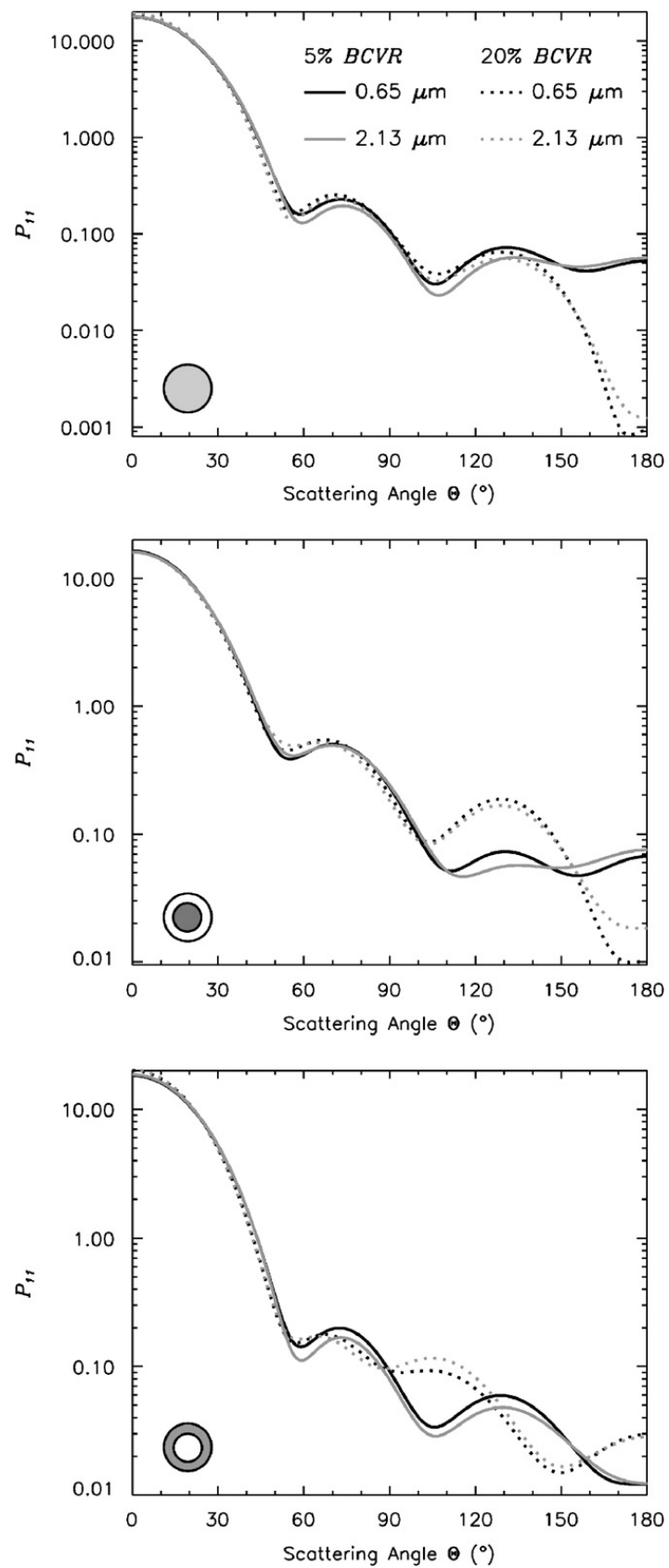
Fig. 5. Phase function as a function of scattering angle at 0.65 and 2.13 μm with a size parameter of 4.0 for three ice particles (the internal mixture of ice and black carbon, coated soot with ice, and coated ice with black carbon) in young contrails for two black carbon volume ratios of 5% and 20%, respectively.

3. Results

3.1. Single-scattering properties

The single-scattering properties of pure ice crystals, contrail particles, coated soot with ice, and coated ice with black carbon are computed on the basis of the coated-sphere Mie code for spherical particles with diameters in the range of 0.02–4.0 μm. Fig. 2 shows the extinction efficiency Q_{ext}, absorption efficiency Q_{abs}, single-scattering albedo ω, and asymmetry factor g as functions of D at wavelengths 0.65 and 2.13 μm for the four types of ice crystals. The single-scattering properties of the four types of ice crystals show pronounced differences at a wavelength of 0.65 μm. Substantial differences are also found for specific types of ice crystals at a wavelength of 2.13 μm. The internal mixture of the contrail particle results in the strongest absorption efficiency followed by the ice coated with soot and the black carbon coated with ice. The absorption for all carbon–ice combinations exceeds that for pure ice, particularly at 0.65 μm. This feature is also indicated by their ω values that tend to be in the range of 0.6–0.9, while the ω values of pure ice crystals are 1.0 at 0.65 μm for all sizes and at 2.13 μm for particle diameters over 0.5 μm.

The four nonzero phase matrix elements for the four types of ice crystals are shown in Figs. 3 and 4 for 0.65 and 2.13 μm, respectively, at a size parameter of 4. It is evident that the phase matrix elements at 2.13 μm are essentially the same as those at 0.65 μm. In the forward scattering directions ($\Theta < 50°$), the values of P_{11} for the four types of ice crystals are similar. Distinct differences are found in backward scattering directions. The elements of P_{12}, P_{33}, and P_{34} also show pronounced differences.

Since there is no commonly accepted value of the BCVR for young contrail particles and the BCVR depends on the sizes of particles, the influence of the BCVR on the optical properties of ice crystals is investigated. Fig. 5 shows an example for the phase function P_{11} as a function of scattering angle at 0.65 and 2.13 μm with a size parameter of 4.0 for three ice crystals (the internal mixture of ice and black carbon, coated soot with ice, and coated ice with black carbon) for two BCVRs of 5% and 20%. Again, the P_{11} at 0.65 and 2.13 μm have similar features for the same size parameter, which are also shown in Figs. 3 and 4. But the BCVR has a strong effect on the P_{11} at both 0.65 and 2.13 μm, particularly, for backscattering.

3.2. Bulk-scattering properties

Log-normal particle size distributions have been used for ice particles in contrails and aerosols e.g., [36,57], given by

$$N(D) = \frac{N_0}{D\sqrt{2\pi}\ln\sigma}\exp\left[-\frac{(\ln D - \ln D_m)^2}{2(\ln\sigma)^2}\right] \tag{3}$$

where N_0 is the total number, D is the maximum dimension of the ice particle, D_m is the median particle diameter, and σ is the standard deviation. The single-scattering properties are computed for D ranging from 0.02 to 4.0 μm with 200 size bins. Furthermore, we define the effective particle size D_e, following [50,58,59,60,61],

$$D_e = \frac{\sum_{i=1}^{200} D_i^3 N(D_i)\Delta D_i}{\sum_{i=1}^{200} D_i^2 N(D_i)\Delta D_i} \tag{4}$$

Table 2
Bulk scattering properties of ice particles in a young contrail with a $D_e = 1.5$ μm

Ice particles	Wavelength (μm)	Absorption efficiency ($\bar{Q}_{abs}$)	Scattering efficiency ($\bar{Q}_{sca}$)	Extinction efficiency ($\bar{Q}_{ext}$)	Single-scattering albedo ($\bar{\omega}$)	Asymmetry factor ($\bar{g}$)
	0.65	3.39506e-07	3.305950	3.30595	1.000000	0.785125
	2.13	0.00433447	0.641332	0.64567	0.993287	0.684770
	0.65	0.516282	2.59761	3.11389	0.83420	0.843526
	2.13	0.186191	0.699769	0.885960	0.789842	0.688802
	0.65	0.297942	2.839363	3.13731	0.905032	0.801825
	2.13	0.185784	0.688499	0.874283	0.787501	0.634544
	0.65	0.431089	2.86125	3.29234	0.869063	0.862687
	2.13	0.180374	0.680610	0.860984	0.790502	0.701887

where i is the index for the size bin, and ΔD is the bin width. Schörder et al. [17] give several typical ice crystal number size distributions for contrails. The D_e and D_m for a fresh contrail are 1.5 and 1.2 μm, respectively. Here we use these two values to derive the standard deviation σ in Eq. (1), which is 1.35.

The single-scattering properties of ice particles are averaged over the log-normal particle size distribution for computing the bulk-scattering properties at $D_e = 1.5$ μm. The mean scattering efficiency $\bar{Q}_{sca}$, absorption efficiency $\bar{Q}_{abs}$, extinction efficiency $\bar{Q}_{ext}$, single-scattering albedo $\bar{\omega}$, asymmetry factor $\bar{g}$, and the phase matrix elements $\bar{\mathbf{P}}(\Theta)$ are derived via the same formulas used in [61] and [62].

The values of $\bar{Q}_{sca}$, $\bar{Q}_{abs}$, $\bar{Q}_{ext}$, $\bar{\omega}$, and $\bar{g}$ for young contrails composed of the four types of ice crystals are listed in Table 2. Similar to the single-scattering properties shown in Fig. 2, strong absorption is noticed for contrail particles, ice-coated soot, and black-carbon-coated ice though pure ice crystals are relatively nonabsorptive, especially at 0.65 μm. The values of $\bar{g}$ are similar for pure ice crystals, contrail particles, and coated ice with black carbon for 2.13 μm. Furthermore, these values are larger than those for coated soot with ice. The value of $\bar{g}$ for pure ice crystals is close to that for coated soot with ice while the value of $\bar{g}$ for contrail particles is close to that for coated ice with black carbon for 0.65 μm.

Fig. 6 shows the mean phase matrix elements ($\bar{P}_{11}$, $\bar{P}_{12}$, $\bar{P}_{33}$, and $\bar{P}_{34}$) for young contrails with $D_e = 1.5$ μm at a wavelength of 0.65 μm. The mean phase matrix elements for young contrails composed of the four types of ice crystals show significant differences. The differences are also observed in those for the wavelength 2.13 μm shown in Fig. 7, particularly, for $\bar{P}_{11}$, $\bar{P}_{12}$, and $\bar{P}_{34}$.

3.3. Stokes parameters

The bulk-scattering properties are input to the vector radiative transfer model to simulate the Stokes parameters (I, Q, U, V) above young contrails composed of the four types of ice crystals. The incident natural sunlight is unpolarized
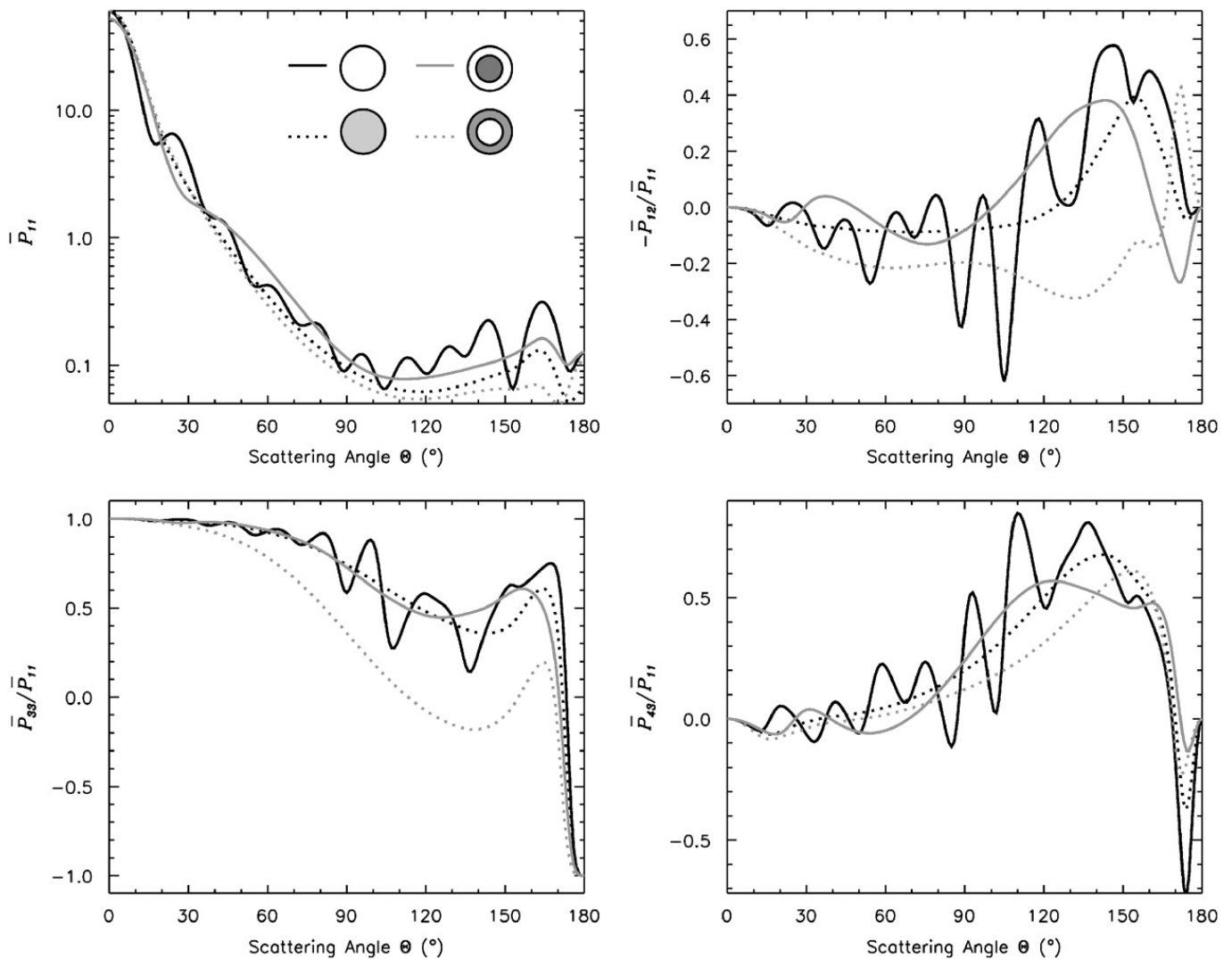
Fig. 6. Mean phase matrix as a function of scattering angle at 0.65 μm for a young contrail with an effective particle size of 1.5 μm.
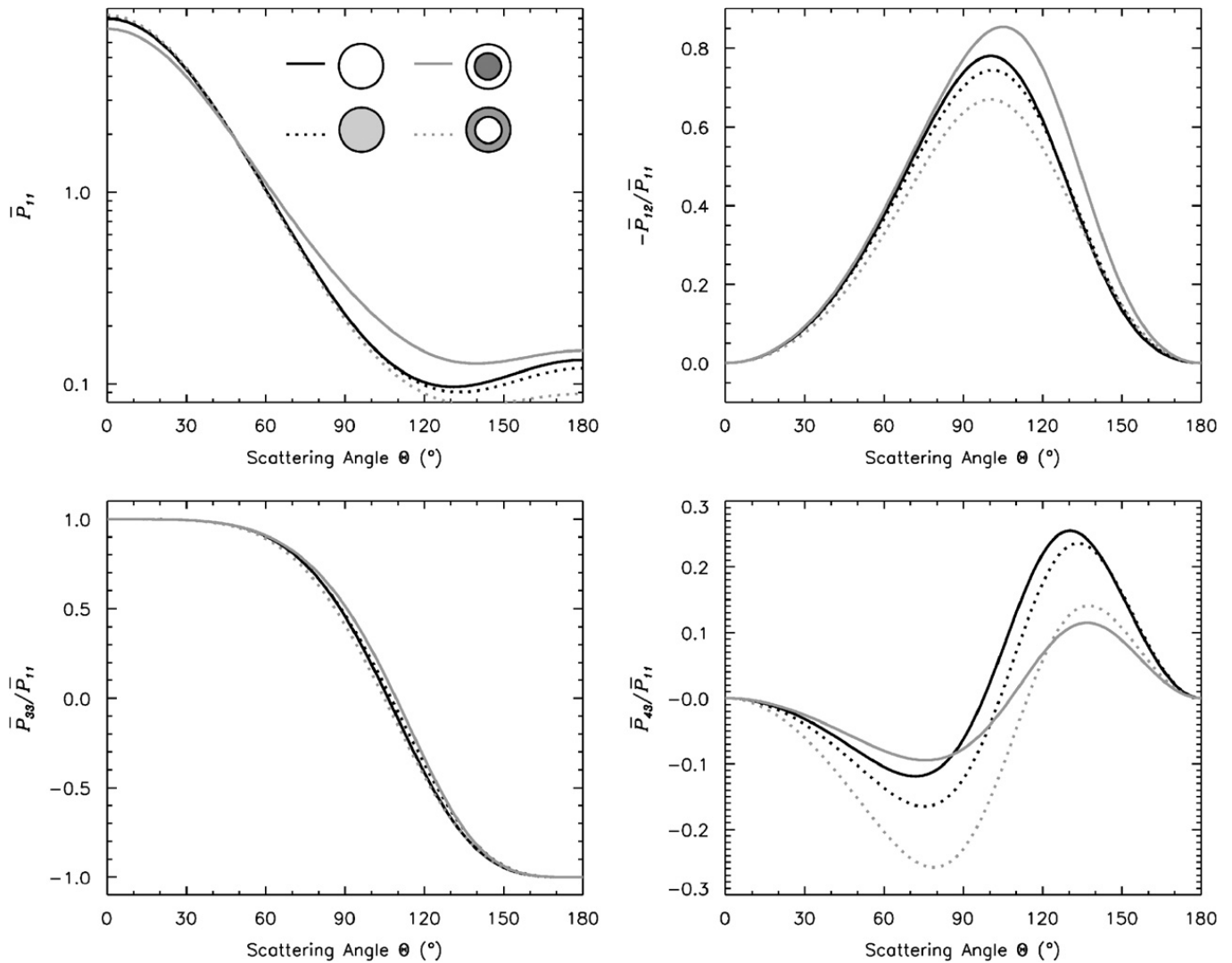
Fig. 7. Same as Fig. 6, but for 2.13 μm.

with $(I_0, Q_0, U_0, V_0) = (1, 0, 0, 0)$. The incident zenith angle is set at 30°. The relative azimuth angle between the incident and scattered radiation beams varies from 0° to 360°. The viewing zenith angle ranges from 0° to 80°. The surface is assumed to be Lambertian with an albedo of 0.1.

The optical thicknesses of contrails vary typically between 0.1 and 0.5 e.g., [4–6,13,19,63]. The lowest observed value of contrail optical thickness is 3.0×10^{-5} [17]. Larger values of optical thickness, >1.0, were also found at higher temperatures (up to $-30\,°C$) [11].

In the present study, the optical thickness of 0.3 at a visible wavelength is used for the young contrail for simulations of the Stokes parameters associated with a young contrail. An optical thickness of 0.3 at the visible wavelength is converted to that at 2.13 μm on the basis of the following relationship:

$$\tau(2.13) = \tau(0.65)\frac{\bar{Q}_{ext}(2.13)}{\bar{Q}_{ext}(0.65)} \tag{5}$$

where $\tau(0.65)$ is the optical thickness of contrails at a visible $(0.65\,\mu m)$ wavelength, i.e., 0.3 used in the present study, $\tau(2.13)$ is the optical thickness of contrails at wavelength 2.13 μm, and $\bar{Q}_{ext}(0.65)$ and $\bar{Q}_{ext}(2.13)$ are the mean extinction efficiencies (Table 2) at 0.65 and 2.13 μm, respectively.

Fig. 8 shows the simulated Stokes parameters associated with the contrails at a wavelength of 0.65 μm. The Stokes parameters for the four types of ice crystals have distinct differences in patterns and values. The values of the Stokes parameters Q, U, and V are smaller than those of I with an order magnitude of 1–4. Each of the Stokes parameters for wavelength 2.13 μm (Fig. 9) have similar patterns, but slightly different values, for the four types of ice crystals.
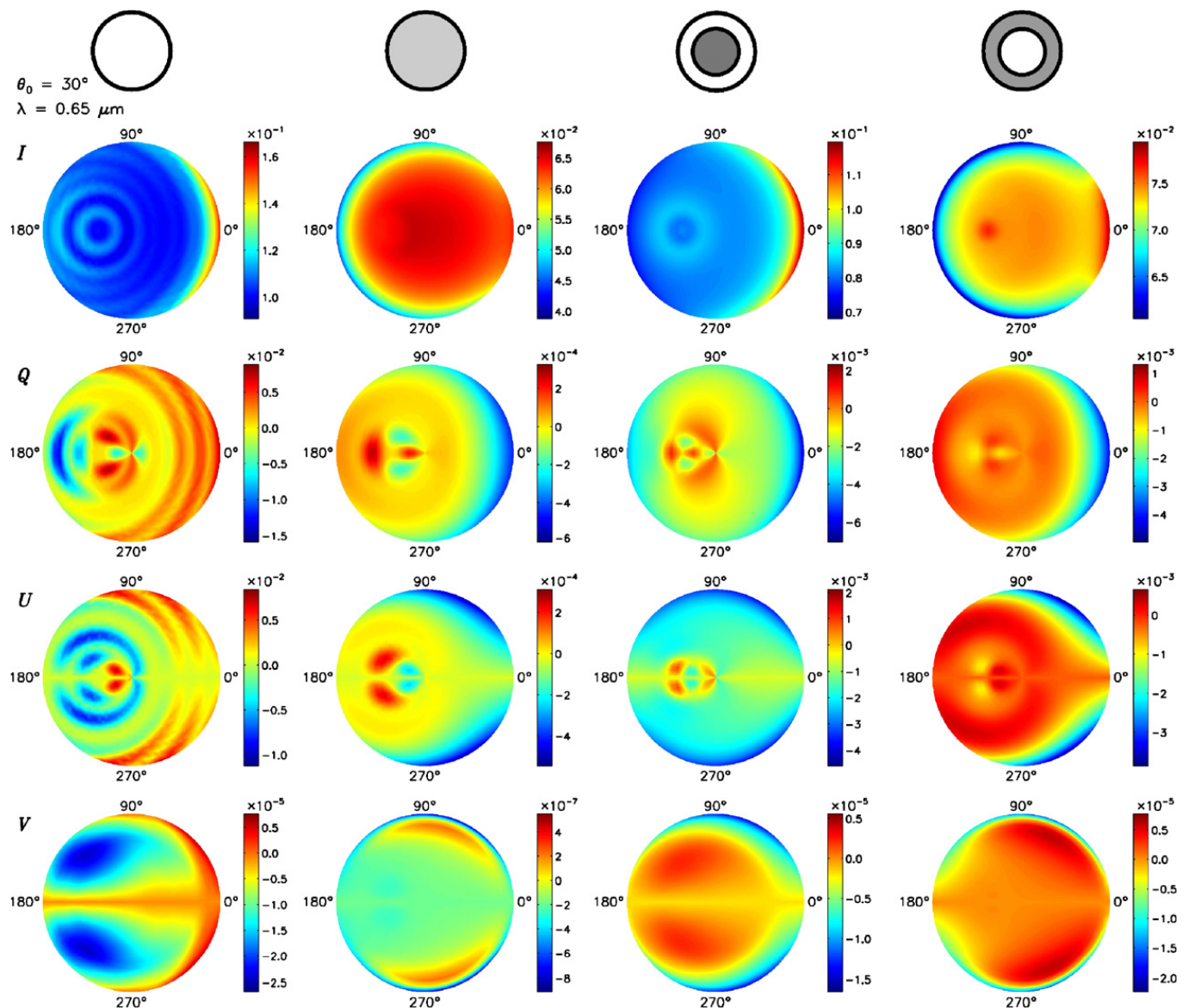
Fig. 8. Simulated stokes parameters (*I*, *Q*, *U*, and *V*) by young contrails composed of the four types of ice crystals considered in the present study for the wavelength 0.65 μm.

4. Summary

The single-scattering properties of ice crystals in contrails are fundamental to the radiative transfer in contrails and remote sensing of the microphysical and optical properties of these clouds. Four types of ice crystals, including pure ice crystals, contrail particles with an internal mixture of pure ice and black carbon, coated soot with ice, and coated ice with black carbon, have been found in young contrails. In this study, the single-scattering properties (absorption efficiency, extinction efficiency, single-scattering albedo, asymmetry factor, and scattering phase matrix) of the four types of ice crystals with maximum dimensions ranging from 0.02 to 4.0 μm are computed from the Wiscombe Mie code for coated spheres at wavelengths 0.65 and 2.13 μm. The single-scattering properties of the four types of ice crystals show pronounced differences. Ice crystals including black carbon have significant absorption efficiencies in comparison with the pure ice crystals. The optical properties of ice crystals with an internal mixture of ice and black carbon and those of soot-coated particles are also found to vary with the black carbon volume ratio.

The single-scattering properties are averaged over a typical log-normal ice particle size distribution for a young contrail to derive the bulk-scattering properties of the young contrail. Similar to the single-scattering properties, pronounced differences are also found for the bulk-scattering properties of contrails composed of the four types of ice crystals. The embedded black carbon strongly increases the absorption of contrail particles, coated ice with black carbon, and coated soot with ice at wavelengths 0.65 and 2.13 μm.
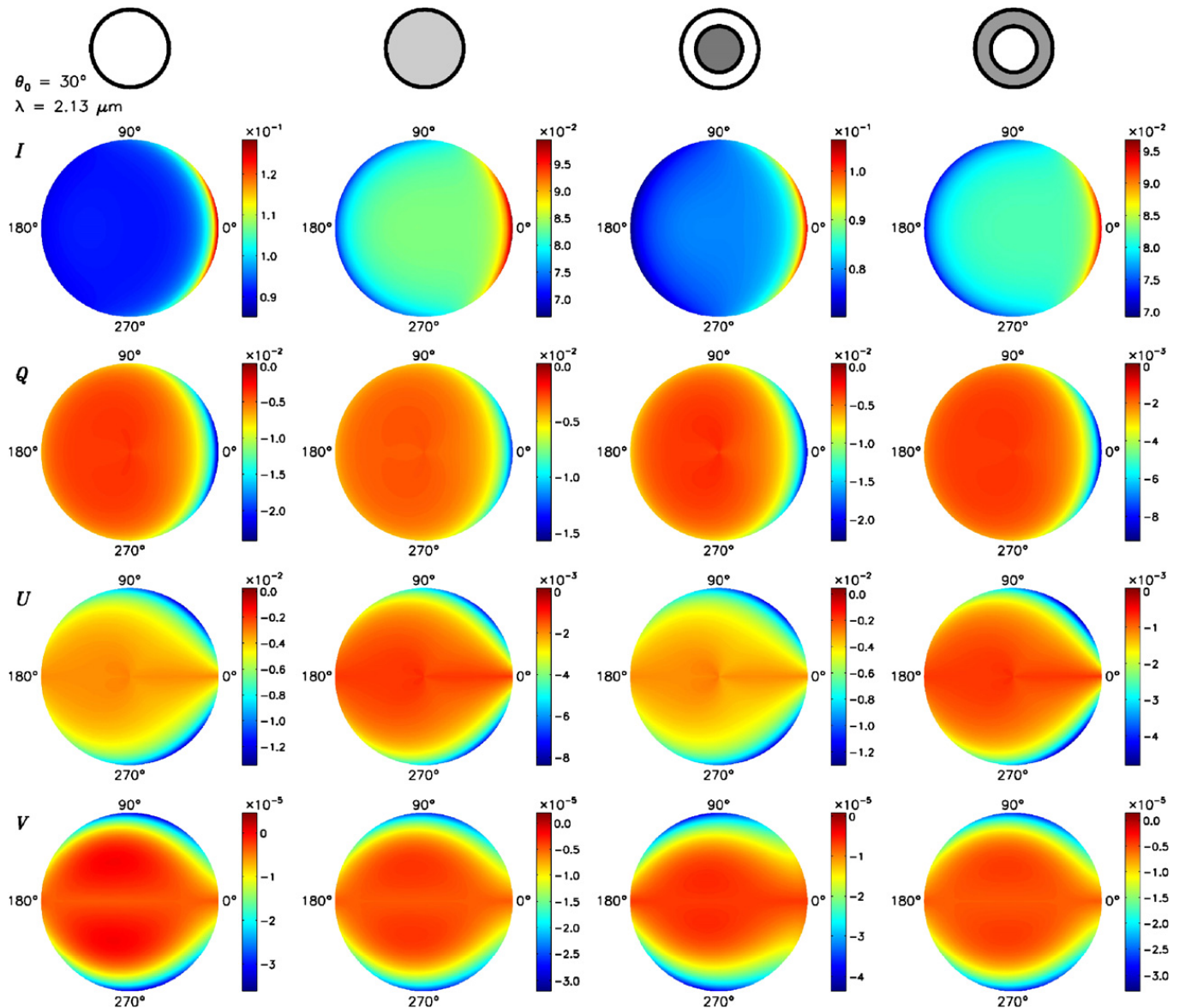
Fig. 9. Same as Fig. 8 but for 2.13 μm.

A rigorous vector radiative transfer model developed by [51] is employed to simulate the full Stokes parameters by young contrails consisting of the four types of ice crystals. The simulated Stokes parameters for the contrails at the wavelength 0.65 μm distinctly vary with viewing zenith and relative azimuth angles. The variations are evident in both patterns and values. However, each of the Stokes parameters for the wavelength 2.13 μm shows similar patterns for the four types of ice crystals although their values are slightly different.

Natural cirrus particles are essentially pure ice particles and differ from those contaminated with carbon in terms of their polarization and spectral signatures. However, the carbon-contaminated particles grow quickly. It is difficult to apply their polarization and spectral signatures to detect young contrails from satellite imagers. With the aging of contrails, the particles within contrails grow to various shapes and sizes. The optical properties of aged, large, and nonspherical particles of contrails deserve future studies to overcome the misidentification of many cirrus streamers as contrails e.g., [63].

Acknowledgments

References

[1] IPCC Climate change 2007: The physical science basis. Contribution of working group I to the fourth assessment report of the intergovernmental panel on climate change, 2007.

[2] Minnis P, Ayers JK, Palikonda R, Phan D. Contrails, cirrus trends, and climate. J Climate 2004;17:1671–85.

[3] Minnis P, Schumann U, Doelling DR, Gierens K, Fahey D. Global distribution of contrail radiative forcing. Geophys Res Lett 1999;26:1853–6.

[4] Myhre G, Stordal F. Global sensitivity experiments of the radiative forcing due to mineral aerosols. J Geophys Res 2001;106:18193–204.

[5] Ponater M, Marquart S, Sausen R. Contrails in a comprehensive global climate model: parameterisation and radiative forcing results. J Geophys Res 2002;107.

[6] Stuber N, Forster PM. The impact of diurnal variations of air traffic on contrail radiative forcing. Atmos Chem Phys 2007;7:3153–62.

[7] Atlas D, Wang Z, Duda DP. Contrails to cirrus-morphology, microphysics, and radiative properties. J Appl Meteor Clim 2006;45:5–19.

[8] Kärcher B, Peter TH, Biermann UM, Schumann U. The initial composition of jet condensation trails. J Atmos Sci 1996;53:3066–83.

[9] Jensen EJ, Ackerman AI, Stevens DE, Toon OB, Minnis P. Spreading and growth of contrails in a sheared environment. J Geophys Res 1998;103:31557–67.

[10] Gothe MB, Grassl H. Satellite remote sensing of the optical depth and mean crystal size of thin cirrus and contrails. Theor Appl Climatol 1993;48:101–13.

[11] Gayet J-F, Febvre G, Brogniez G, Chepfer H, Renger W, Wendling P. Microphysical and optical properties of cirrus and contrails: cloud field study on 13 October 1989. J Atmos Sci 1996;53:126–38.

[12] Petzold A, et al. Near field measurements on contrail properties from fuels with different sulfur content. J Geophys Res 1997;102:29,867–80.

[13] Minnis P, Young DF, Garber DP, Nguyen L, Smith Jr WL, Palikonda R. Transformation of contrails into cirrus during success. Geophys Res Lett 1998;25:1157–60.

[14] Ström J, Ohlsson S. In situ measurements of enhanced crystal number densities in cirrus clouds caused by aircraft exhaust. J Geophys Res 1998;103:11355–61.

[15] Kuhn M, Petzold A, Baumgardner D, Schröder F. Particle composition of a young condensation trail and of upper tropospheric aerosol. Geophys Res Lett 1998;25:2679–82.

[16] Chylek P, Hallett J. Enhanced absorption of solar radiation by cloud droplets containing soot particles in their surface. Q J R Meteor Soc 1992;118:167–72.

[17] Schörder F, Kärcher B, Duroure C, Ström J, Petzold A, Gayet J-F, et al. On the transition of contrails into cirrus clouds. J Atmos Sci 2000;57:464–80.

[18] Kärcher B, Möhler O, DeMott PJ, Pechtl S, Yu F. Atmospheric chemistry and physics insights into the role of soot aerosols in cirrus cloud formation. Atmos Chem Phys 2007;7:4203–27.

[19] Meerkötter R, Schumann U, Doelling DR, Minnis P, Nakajima T, Tsushima Y. Radiative forcing by contrails. Ann Geophys 1999;17:1070–84.

[20] Chylek P, Videen G, Ngo D, Pinnick RG, Klett JD. Effect of black carbon on the optical properties and climate forcing of sulfate aerosols. J Geophys Res 1995;100:16325–32.

[21] Clarke AD, et al. Size distributions and mixtures of dust and black carbon aerosol in Asian outflow: physiochemistry and optical properties. J Geophys Res 2004;109:D15S09.

[22] Mishchenko MI, Liu L, Travis LD, Lacis AA. Scattering and radiative properties of semi-external versus external mixtures of different aerosol types. JQSRT 2004;88:139–47.

[23] Mackowski DW. A simplified model to predict the effects of aggregation on the absorption properties of soot particles. JQSRT 2006;100:237–49.

[24] Liu L, Mishchenko MI. Effects of aggregation on scattering and radiative properties of soot aerosols. J Geophys Res 2005;110:D11211.

[25] Liu L, Mishchenko MI. Scattering and radiative properties of complex soot and soot-containing aggregate particles. JQSRT 2007;106:262–73.

[26] Danielson R, Moore D, van de Hulst H. The transfer of visible radiation through clouds. J Atmos Sci 1969;26:1078–87.

[27] Chylek P, Lesins GB, Videen G, Wong JGD, Pinnick RGD, Ngo D, Klett JD. Black carbon and absorption of solar radiation by clouds. J Geophys Res 1996;101:23365–72.

[28] Chylek P, Ramaswamy V, Cheng RJ. Effect of graphitic carbon on the albedo of clouds. J Atmos Sci 1984;41:3076–84.

[29] Chylek P, Videen G, Geldart DJW, Dobbie JS, Tso HCW. Effective medium approximations for heterogeneous particles. In: Mishchenko MI, Hovenier JW, Travis LD, editors. Light scattering by nonspherical particles: theory, measurements, and applications. San Diego: Academic Press; 2000. p. 273–308.

[30] Twohy CH, Clarke AD, Warren SG, Radke LF, Charlson RJ. Light-absorbing material extracted from cloud droplets and its effect on cloud albedo. J Geophys Res 1989;94:8623–31.

[31] Macke A, Mishchenko MI, Cairns B. The influence of inclusions on light scattering by large ice particles. J Geophys Res 1996;101:23311–6.

[32] Liu L, Mishchenko MI, Menon S, Macke A, Lacis AA. The effect of black carbon on scattering and absorption of solar radiation by cloud droplets. JQSRT 2002;74:195–204.

[33] Yang P, et al. Inherent and apparent scattering properties of coated or uncoated spheres embedded in an absorbing host medium. Appl Opt 2002;41:2740–59.

[34] IPCC. Special report on aviation and the global atmosphere. In: Penner JE, Lister DH, Griggs DJ, Dokken DJ, McFarland M, editors. Intergovernmental panel on climate change. New York, USA: Cambridge University Press; 1999.

[35] Warren SG. Optical constants of ice from ultraviolet to the microwave. Appl Opt 1984;23:1206–25.

[36] Levoni C, Cervino M, Guzzi R, Torricella F. Atmospheric aerosol optical properties: a database of radiative characteristics for different components and classes. Appl Opt 1997;36:8031–41.

[37] Kattawar GW, Hood DA. Electromagnetic scattering from a spherical polydispersion of coated spheres. Appl Opt 1976;15:1996–9.

[38] Toon OB, Ackerman TP. Algorithms for the calculation of scattering by stratified spheres. Appl Opt 1981;20:3657–60.

[39] Bohren CF, Huffman DR. Absorption and scattering of light by small particles. New York: Wiley; 1983. p. 530.

[40] Kaiser T, Schweiger G. Stable algorithm for the computation of Mie coefficients for scattered and transmitted fields of a coated sphere. Comput Phys 1993;7:682–6.

[41] Fuller KA. Scattering of light by coated spheres. Opt Lett 1993;18:257–9.

[42] Mishchenko MI, Hovenier JW, Travis LD. Light scattering by nonspherical particles: theory, measurements, and applications. San Diego: Academic Press; 2000.

[43] Fuller KA, Mackowski DW. Electromagnetic scattering by compounded spherical particles. In: Mishchenko MI, Hovenier JW, Travis LD, editors. Light scattering by nonspherical particles: theory, measurements, and applications. San Diego: Academic Press; 2000. p. 225–72.

[44] Van de Hulst HC. Light scattering by small particles. Mineola, New York: Dover; 1957. 470pp.

[45] Freudenthaler V, Homburg F, Jäger H. Optical parameters of contrails from lidar measurements: linear depolarization. Geophys Res Lett 1996;23:3715–8.

[46] Sassen K, Hsueh C. Contrail properties derived from high-resolution polarization lidar studies during SUCCESS. Geophys Res Lett 1998;25:1165–8.

[47] Mishchenko MI, Sassen K. Depolarization of lidar returns by small ice crystals: an application to contrails. Geophys Res Lett 1998;25:309–12.

[48] Kattawar GW, Plass GN. Radiance and polarization of multiple scattered light from haze and clouds. Appl Opt 1968;7:1519–27.

[49] Davis C, Emde C, Harwood R. A 3-D polarized reversed Monte Carlo radiative transfer model for millimeter and submillimeter passive remote sensing in cloudy atmospheres. IEEE Trans Geosci Remote Sens 2005;43:1096–101.

[50] Hansen JE, Travis LD. Light scattering in planetary atmospheres. Space Sci Rev 1974;16:527–610.

[51] de Haan JF, Bosma PB, Hovenier JW. The adding method for multiple scattering calculations of polarized light. Astron Astrophys 1987;183:371–91.

[52] Evans KF, Stephens GL. A new polarized atmospheric radiative transfer model. JQSRT 1991;46:413–23.

[53] Weng F. A multi-layer discrete-ordinate method for vector radiative transfer in a vertically-inhomogeneous, emitting and scattering atmosphere I: Theory. JQSRT 1992;47:19–33.

[54] Weng F. A multi-layer discrete-ordinate method for vector radiative transfer in a vertically-inhomogeneous, emitting and scattering atmosphere II: Application. JQSRT 1992;47:35–42.

[55] Schulz FM, Stamnes K, Weng F. VDISORT: an improved and generalized discrete ordinate method for polarized (vector) radiative transfer. JQSRT 1999;61:105–22.

[56] Vermote EF, Tanre D, Deuze JL, Herman M, Morcrette JJ. Second simulation of the satellite signal in the solar spectrum, 6S: An overview. IEEE Trans Geosci Remote Sens 1997;35:675–86.

[57] Gierens KM, Ström J. A numerical study of aircraft wake induced ice cloud formation. J Atmos Sci 1998;55:3253–63.

[58] Foot JS. Some observations of the optical properties of clouds. Part II: Cirrus. Q J R Meteorol Soc 1988;114:145–64.

[59] King MD, Platnick S, Yang P, Arnold GT, Gray MA, Riédi JC, et al. Remote sensing of liquid water and ice cloud optical thickness, and effective radius in the arctic: application of airborne multispectral MAS data. J Atmos Ocean Technol 2004;21:857–75.

[60] Baum BA, Heymsfield AJ, Yang P, Bedka ST. Bulk scattering properties for the remote sensing of ice clouds. Part I: Microphysical data and models. J Appl Meteorol 2005;44:1885–95.

[61] Yang P, Wei H, Huang H-L, Baum BA, Hu YX, Kattawar GW, et al. Scattering and absorption property database for nonspherical ice particles in the near-through far-infrared spectral region. Appl Opt 2005;44:5512–23.

[62] Hong G. Parameterization of scattering and absorption properties of nonspherical ice crystals at microwave frequencies. J Geophys Res 2007; 112:D11208.

[63] Minnis P, Palikonda R, Walter BJ, Ayers JK, Mannstein H. Contrail properties over the eastern North Pacific from AVHRR data. Meteorol Z 2005; 14:515–23.